COBEM2015

ABCM Associação Brasileira de Engenharia e Ciências Mecânicas

23rd ABCM International Congress of Mechanical Engineering
December 6-11, 2015, Rio de Janeiro, RJ, Brazil

Characterizing the Vibrational Modes of a Cavitating Bubble Immersed in a Magnetic Fluid

Sara Malvar
Rafael Gabler Gontijo
Francisco Ricardo Cunha

University of Brasília, Department of Mechanical Engineering, Fluid Mechanics of Complex Flows Lab - VORTEX, Brasília - DF, Brazil 70910 900
malvar.sara@gmail.com
rafaelgabler@gmail.com
frcunha@unb.br

Abstract. *The main goal of this article is to identify the vibrational patterns of an oscillating spherical bubble immersed in a ferrofluid using Neural Networks. The gas bubble is immersed on a magnetic fluid and subjected to an harmonic pressure excitation and an applied magnetic field. The classical Rayleigh-Plesset equation is modified and a magnetic version is proposed in order to model the radial motion of the bubble. Being a very non-linear system, the correct identification of the vibrational patterns is not possible using linear system tools. In this case, fuzzy logic and neural networks are a good solution for the correct pattern identification. The magnetic version of Rayleigh-Plesset equation is a second order non linear ordinary differential equation and it is solved through a fifth order Runge-Kutta scheme with adaptive time step. Four different vibrational patterns are identified and proposed regarding its frequency response and Lyapunov exponets. Based on the Lyapunov exponents it is possible to analyze its non-chaotic behavior. Those Lyapunov exponents are used in a backpropagation neural network to correctly identify the bubble vibration modes what could lead to the identification of the flow physical parameters in practical applications. In order to compare the performance, another neural network is trainned with the amplitude and frequency information of the bubble motion from $\omega = 0$ to $\omega = 10$, based on its Fast Fourier Transform. The new results are compared with previous simulations made with harmonic response in frequency spectrum, in which only the first harmonic was considered.*

Keywords: *bubble dynamics, nonlinear dynamics, neural networks, cavitation, ferrofluids*

1. INTRODUCTION

Since the early work of Rayleigh, the dynamics of cavities in general and bubbles in particular, have acquired a respectable place in cavitation research (Chahine, 1982). In many applications it is of absolute necessity to control the collapse of the bubbles, thus avoiding erosion. On the other hand, in medical applications, the collapse of microbubbles may be necessary, in order to kill cancer cells (Zharov *et al.*, 2005).

In this context, the need to control the bubble's motion and its collapse lead us to use a ferrofluid. Ferrofluids are synthesized as a stable colloidal suspensions of ferromagnetic grains (Bacri and Salin, 1982) in a non-magnetic carrier liquid. Brownian motion keeps the nanoscopic particles from settling under gravity, and a surfactant layer, such as oleic acid, or a polymer coating surrounds each particle to provide short range steric hindrance and electrostatic repulsion between particles preventing particle agglomeration (Odenbach, 2002). This coating allows ferrofluids to maintain fluidity even in intense high-gradient magnetic fields (Bolshakova *et al.*, 2005). Ferrofluids also have very interesting lines, patterns, and structures that can develop from ferrohydrodynamic instabilities (Zahn, 2001). In this context, the application of a magnetic field can control the fluid flow or a immersed bubble, for example.

We consider that the bubble motion is only radial. This assumption is valid when the bubble is very small and its surface tension is large, preventing tangential deformation, as seen in figure 1. It is noteworthy that this model is not valid during the collapse, at which point the bubble undergoes several deformations in form (Johnsen and Colonius, 2009).

Regarding practical applications of magnetic suspensions, we may say that they started to be explored by physicists and engineers due to its wide range of applications (Gontijo and Cunha, 2015). This particulate suspensions have been used in the study of capillary ascension (Bashtovoi *et al.*, 2002), magnetic convection (Gontijo and Cunha, 2012) and in the magnetodydrodynamic thermochemotherapy field (Brusentsov *et al.*, 2008) in which the use of bio-compatible magnetic fluid is studied for the treatment of tumors.

Based on this, we note that the oscillatory behavior of the bubble can be controlled by application of a magnetic field

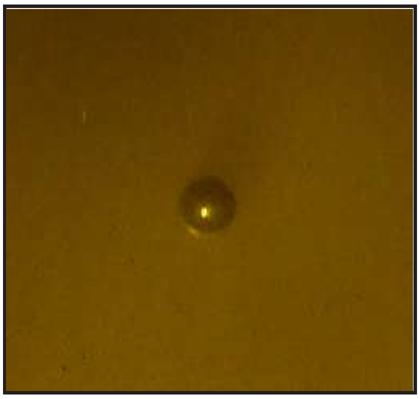

Figure 1: Microbubble with diameter of $d = 1.6mm$ immersed in a ferrofluid (mixture of EFH3, a commercial ferrofluid manufactured by Ferrotec, and mineral oil with particle volume fraction of $\approx 252.86ppm$).

(Cunha *et al.*, 2002). In this context, new vibrational patterns are identified. With that said, it is possible to propose a system to identify these pattern during an experiment or pratical application. In this case, an oscillating bubble could have its vibrational pattern identified with the use of neural networks trainned for pattern recognition. The ability of a neural network to approximate any complex functional relationship makes the selection of a suitable regression equation for particular application unnecessary. Artificial neural networks are inherently parallel and have the capability to learn non-linear relationships, which may exist between a set of inputs and outputs.

In the present study, we used a sinusoidal excitation with variable amplitude and frequency forcing and a constant magnetic field to study the oscillation of a microbubble immersed on a superparamagnetic ferrofluid. With the characterization of the nonlinear system, proposed as the mgnetic version of Rayleigh-Plesset equation, it is possible to controll the bubble motion. For this end, two neural networks are trainned in order to idenfity the bubble vibrational modes. In this context, it is possible to compare which dynamical tool (Lyapunov exponents or frequency spectrum) is better to train the neural network.

2. MATHEMATICAL MODELLING

The complete problem of a gas bubble undergoing nonlinear radial pulsations in a ferrofluid is a complex problem. The main governing equations used in the mathematical modeling of the problem are based on the principle of mass conservation (continuity equation), linear momentum balance (Newton's second law - equation of motion), Gauss law of magnetism (absence of magnetic monopoles) and Ampère-Maxwell equation for a non-conducting fluid (magnetostatic limit).

Consider a spherical bubble immersed in a magnetic fluid of viscosity μ and density ρ, as shown in figure (2). The inner side of the bubble is composed by a mixture of contaminant gas (which develops a polytropic process) and liquid vapour. Therefore, quantities like pressure gradients in the liquid or surfactants in the fluid are neglected. Changes in the vapour temperature may modify its density modifying the bubble dynamics (Soh and Karimi, 1996). However, for a small equilibrium vapour density the isothermal process is valid (Brujan, 1999).

The balance of mass for an incompressible fluid written in spherical coordinates is given by

$$\frac{1}{r}\left[\frac{\partial}{\partial r}(r^2 u_r)\right] = 0 \rightarrow \int \frac{\partial}{\partial r}(r^2 u_r) dr = 0, \tag{1}$$

where r represents the physical distance of the bubble center and a point in the fluid, u_r is the radial component of the Eulerian velocity field. Integrating equation (1) from the surface of the bubble with radius R to an arbitrary point in the liquid (distance r) we have, after some algebric manipulations:

$$u(r,t) = \frac{R^2}{r^2}\frac{dR}{dt} = \frac{R^2}{r^2}\dot{R}, \tag{2}$$

which gives the velocity information at any point of the liquid. The balance of momentum for the non-Newtonian fluid flow can be written as

$$\rho\left(\frac{\partial \boldsymbol{u}}{\partial t} + \boldsymbol{u}\cdot\nabla\boldsymbol{u}\right) = -\nabla p + \nabla\cdot\boldsymbol{\sigma^N} + \nabla\cdot\boldsymbol{\sigma}, \tag{3}$$

where $\boldsymbol{\sigma^N}$ represents the Newtonian contibution of the stress tensor, while $\boldsymbol{\sigma}$ is used to denote the non-Newtonian fluid

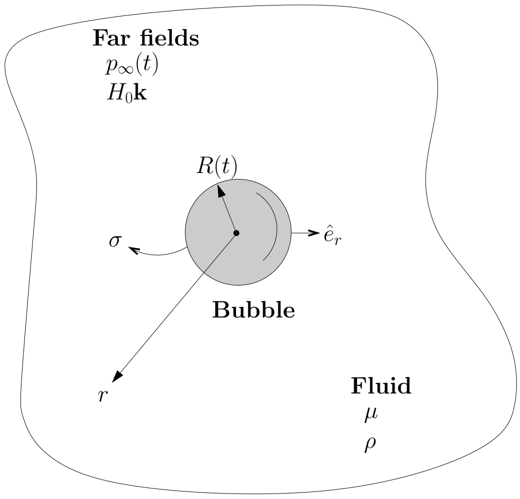

Figure 2: Schematic of a gas bubble immersed in a magnetic fluid of viscosity μ and density ρ with acoustic and magnetic applied fields.

effects, $\boldsymbol{u}$ is the Euleurian velocity field and rho is the fluid density. Writting the radial component of Cauchy equation in spherical coordinates with non-Newtonian stress tensor, we have:

$$\rho\left(\frac{\partial u}{\partial t}+u\frac{\partial u}{\partial r}\right)=-\frac{\partial p}{\partial r}+\frac{1}{r^2}\frac{\partial}{\partial r}(r^2\sigma_{rr}^N)+\frac{1}{r^2}\frac{\partial}{\partial r}\left(r^2\sigma_{rr}\right)-\frac{(\sigma_{\theta\theta^N}+\sigma_{\phi\phi^N})}{r}-\frac{(\sigma_{\theta\theta}+\sigma_{\phi\phi})}{r} \tag{4}$$

$\sigma_{rr}^N+\sigma_{\phi\phi}^N+\sigma_{\theta\theta}^N=0$, equation (4) can be written using $\sigma_{rr}^N=-\sigma_{\theta\theta}^N-\sigma_{\phi\phi}^N$. The effects of the ϕ component will be neglected in the next steps. Integrating in the flow domain, represented by $R\leq r\leq\infty$, we have:

$$\int_R^\infty\frac{2\dot{R}^2R+R^2\ddot{R}}{r^2}dr-\int_R^\infty\frac{2\dot{R}^2R^4}{r^5}dr=-\frac{1}{\rho}\int_R^\infty\frac{\partial p}{\partial r}dr+\frac{1}{\rho}\int_R^\infty\frac{2\partial\sigma_{rr}}{r}dr+\int_R^\infty\frac{\partial\sigma_{rr}}{\partial r}dr-\frac{1}{\rho}\int_R^\infty\frac{\sigma_{\theta\theta}}{r}dr \tag{5}$$

In the study of magnetic fluid, Maxwell's laws in the magnetostatic limit should be applied. In other words, the magnetic effect related to the movement of electric charges may be neglected and so does the electric field involved. Said that, the Gauss's law of magnetism states that the magnetic induction flow through a closed surface is zero and the rotational of the applied magnetic field is null.

Maxwell stress tensor for magnetic fluids is given by:

$$\boldsymbol{\sigma}=\left(-\frac{\mu_0H^2}{2}\right)\boldsymbol{I}+\boldsymbol{HB}, \tag{6}$$

in this case, both tangential and radial components are given by (Rosensweig, 1987):

$$\sigma_{rr}^{mag}=\frac{-\mu_0}{2}(H_r^2+H_\theta^2)+\mu(1+\chi)H_r^2 \tag{7}$$

$$\sigma_{\theta\theta}^{mag}=\frac{-\mu_0}{2}(H_r^2+H_\theta^2)+\mu(1+\chi)H_{\theta\theta}^2, \tag{8}$$

here we use the fact that $\boldsymbol{B}=\mu_0\left(\boldsymbol{M}+\boldsymbol{H}\right)$, where μ_0 is the magnetic permeability of the free space and $\boldsymbol{M}$ is the fluid magnetization, which in this case is assumed to be aligned with the applied field, so $\boldsymbol{M}=\chi\boldsymbol{H}$, where χ is the magnetic suceptibility of the fluid (superparamagnetism hypothesis). Whereas the bubble is a curved interface between two fluids, there is a normal stress discontinuity in the interface due to its surface tension.

The applied magnetic field is also given by (Rosensweig, 1987):

$$\boldsymbol{H}=\left\{\begin{array}{c}-A(cos\theta\hat{e}_r-sin\theta\hat{e}_\theta),\text{ for }r<R\\-(C-\frac{2D}{r^3})cos\theta\hat{e}_r+(C+\frac{D}{r^3})sin\theta\hat{e}_\theta,\text{ for }r>R\end{array}\right. \tag{9}$$

The magnetic field far from the sphere should approach the uniform applied field $H_0\boldsymbol{k}$ in which $\boldsymbol{k}$ is the unitary vector in the z direction. In spherical coordinates, $\boldsymbol{k}=\hat{e}_rcos\theta-\hat{e}_\theta sin\theta$, so considering $r\longrightarrow\infty$, we have

$$C=-H_0 \qquad A=\frac{-3\mu_1H_0}{\mu_r+2\mu_1} \qquad D=\frac{\mu_2-\mu_1}{\mu_2+2\mu_1}R^3H_0 \tag{10}$$

As the bubble is a curved interface between two immiscible fluids, there is a normal stress discontinuity in the interface due to its surface tension. The jump of normal stresses is given by Young-Laplace equation (Young, 1805; Laplace, 1805):

$$\Sigma_{rr,\ell} - \Sigma_{rr,b} = \frac{2\tilde{\sigma}}{R} - \sigma_{rr}^{mag}|_{r=R}, \tag{11}$$

where $\tilde{\sigma}$ represents the surface tension coefficient and $\Sigma_{rr,\ell}$ and $\Sigma_{rr,b}$ denote the radial component of the traction for the liquid side and the bubble inner side, respectively. Since the magnetic field has already decreased to zero in $r = R$, $\sigma_{rr}^{mag}|_{r=R} = 0$. The pressure inside the bubble is given by $p_b(t) = p_v + p_g(t)$, where p_v is the liquid vapour pressure and $p_g(t)$ refers to the gas pessure (considered to be part of a polytropic process). After some manipulation and considering the excitation pressure as $p_\infty = 1 + \varepsilon sin(\omega t)$, it is possible to write the magnetic version of Rayleigh-Plesset equation in its non-dimensional form as

$$\ddot{R}^* R^* + \frac{3}{2}\dot{R}^{2*} = \frac{2}{We}\left[-\frac{1}{R^*} + \left(\frac{1}{R^*}\right)^{3n}\right] + \left(\frac{1}{R^*}\right)^{3n} - \varepsilon^* sin(\omega^* t^*) - 1 - \frac{4}{Re}\frac{\dot{R}^*}{R^*} + \\ + \frac{1}{Re^{mag}}\left\{\frac{\chi}{2}\left[ln\left(\frac{R^*_\infty}{R^*}\right) - \frac{C_1}{2}\right] - \frac{C_1}{8}\right\}, \tag{12}$$

where

$$Re = \frac{\rho U_c R_E}{\mu} \quad \text{and} \quad We = \frac{\rho U_c^2 R_E}{\sigma_s} \tag{13}$$

Here, Re corresponds to the Reynolds number (i.e. the relation between inertial and viscous forces) and We is the Weber number, which denotes the ratio of inertial and surface tension forces. C_1 and Re^{mag} are given respectively by:

$$C_1 = \frac{3}{4} \quad \text{and} \quad Re^{mag} = \frac{\rho U_c^2}{\mu_0 H_0^2} \tag{14}$$

In equation, the physical non-dimensional parameter Re_{mag} is called in the present work as being the magnetic Reynolds number. This parameter measures the relative importance between inertial and magnetic forces.

3. NUMERICAL METHODOLOGY

The governing Equation (12) is strongly nonlinear. In this case, an analystical solution is not available. Therefore, the integration of (12) requires the use of numerical techniques. A Runge-Kutta scheme with an adaptive time step implemented e validated by Malvar *et. al.* (Malvar *et al.*, 2015) will also be used in this work. The adaptive time step is quite useful since it does reduce the computational cost of the code in about 85%. Owing to nonlinearities imposed by the condition of having a magnetic liquid surrounding the bubble, the use of quite small time steps could increase the computational cost. On the other hand, large time steps could filter the details of the bubble oscillations at higher frequencies.

The procedure of the numerical integration is presented in terms of a logical algorithm as follows in (15):

$$\left[\begin{array}{ll}
1. & \text{Define } Re, We, Re_{mag}, \chi, n \text{ (polytropic coefficient) and } \varepsilon; \\
2. & \text{Initial conditions and simulation time } R(0) \text{ and } G(0); \\
3. & \texttt{While } t(i-1) < b \texttt{ do ;} \\
4. & \text{Compute } R_{min}(R(0), We); \\
5. & \text{Compute } k_1, k_2, k_3, k_4, k_5, k_6 \text{ e } q_1, q_2, q_3, q_4, q_5, q_6; \\
6. & \text{Forth order} \rightarrow g(i) \text{ and Fifth order } \rightarrow P(i); \\
7. & \text{Compute } erro = \left|\left(\dfrac{g(i) - P(i)}{tolerance}\right)\right|; \\
8. & \texttt{If } error > 1 \texttt{ then} \rightarrow dt = htemp * seg \\
9. & \texttt{Compute new } k_1, k_2, k_3, k_4, k_5, k_6 \text{ and } q_1, q_2, q_3, q_4, q_5, q_6; \\
10. & \texttt{If } error > 1 \texttt{ then} \rightarrow dt = htemp * seg; \\
11. & \texttt{If } error > parameter \texttt{ then} \rightarrow hnext = seg * htemp * parameter2; \\
12. & \texttt{If } error < parameter \texttt{ then} \rightarrow hnext = htemp * parameter3; \\
13. & \texttt{If } R(i) < R_{min} \texttt{ then} \rightarrow \textbf{ COLAPSE} \\
14. & \texttt{If } hdid < dtm \texttt{ then} \rightarrow \textbf{ END} \\
15. & \texttt{If } hdid > dtm \texttt{ then} \rightarrow \texttt{ go to step 5.}
\end{array}\right. \tag{15}$$

In the scheme shown in (15), b denotes the total time of the simulation , which is an user defined option. The minimum radius, R_{min} represents the minimum radius proposed (Albernaz and Cunha, 2011) where the bubble may collapse. The variable $htemp$ detones the temporary time step and the variable $hnext$ is the next time step to be used in the subsequent iteration, after the multiplication by the security parameters (seg) and tolerance ($parameter2$ and $parameter3$). Subsequently, the time step dt becomes $hdid$ at the end of the iteration and it is compared with the minimum time, dtm, defined by the user.

The minimum radius obtained in the eminence of a bubble collapse, which is defined as the bubble quick and sudden contraction, is given by:

$$R_{min} = R_0 e^{-(R_0)^2 \left[\frac{1+R_0\frac{We}{3}}{We+2}\right]}. \tag{16}$$

where R_{min} is the minimum radius, R_0 is the initial radius and We is the Weber number.

4. RESULTS

In this section, we present different vibrational patterns of the nonlinear bubble motion. In order to understand the bubble behavior when immersed in a magnetic fluid analysis such as collapse diagram and vibrational patterns identification must be made. However, we do not intend to characterize all possible vibrational modes of the nonlinear bubble oscillatory motion. The attenuation of collapse can be seen in figure (3). Once the bubble undergoes an external magnetic field, it is possible to analyze how the concept of collapse is modified by studying the collapse diagram. When the applied magnetic field is increased, there is a stabilization on the bubble movement preventing collapse. This results can be indicating that if a magnetic time scale is coupled with the period of bubble oscillations this mechanics produces a stabilization of the system. Actually in the presence of the magnetic field the alignment of the magnetic particle with the field must create a resistance for the radial bubble motion making a substantial attenuation on the amplitude of the oscillations. This depends on how the magnetic relaxation time of the particle or fluid magnetization responds to the field action compared with the period of the bubble oscillation. In general, it seems that the presence of a magnetic field even at moderate Re_{mag} makes the motion of the bubble more stable decreasing the vibrational degree freedom of the bubble motion and avoiding premature collapse.

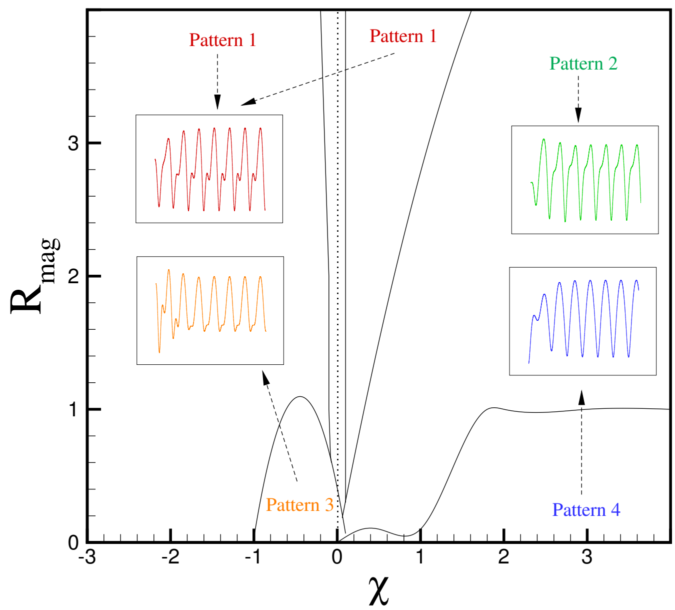

Figure 3: Typical vibration patterns as a function of Re_{mag} and χ identified with the present numerical simulation. For all simulations runs: $Re = 10$, $We = 10$ and $\varepsilon = 0.3$.

These vibrational patterns can be analyzed by different dynamical systems approach of such as Fast Fourier Transform (FFT), Poincaré section, phase plot, Lyapunov exponents and wavelets transform as shown in 4. Each one of these approaches promotes gain of informations when characterizing a nonlinear dynamic system. For instance, the frequency response give us information about the energy stored in every harmonic. Since the excitation frequency used was $\omega = 1$, we note that the biggest amount of energy is present in the first harmonic of a time series. On the other hand, deformations in the time response also can induce spectral spreading in which the energy of the system spreads along different harmonics. That means that in some part of the system response, there is a frequency variation. That frequency variation is also seen in the phase plot as a shape deformation in the limit cycle. In this case, there is no second limit cycle, pointing out that no period doubling is presented. The Poincaré section is another interesting approach to be used, specially when the system is periodic. The stability of a periodic orbit of the original system is closely related to the stability of the fixed point of the corresponding Poincaré map. We can see that there is a difference in the energy levels seen in the phase plot.

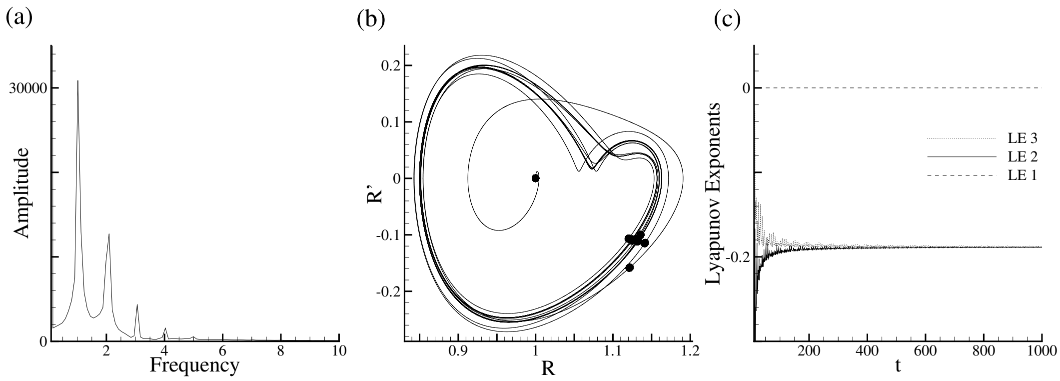

Figure 4: Bubble response using different dynamical system approaches to analysis. (a) Shows the FFT; (b) the phase plot and Poincaré section; (c) shows the three Lyapunov exponents. In all cases $Re = 10$, $We = 10$, $\varepsilon = 0.3$, $\omega = 1$, $\chi = 0.3$ and $Re_{mag} = 1$.

Another way to examine the degree of nonlinearity in a dynamical system is by computing the Lyapunov exponents. This study allows us to observe the system sensitivity to initial conditions and the divergence and convergence rates of nearby trajectories in phase space. This means that that the Lyapunov exponents (LE) or λ represent a measure of the exponential separation (e^{λ}) of the neighbouring trajectories over all points of a trajectory around an attractor. In terms of Kolmogorov entropy (entropic metric) the LE may be interpreted as a mesure of the disorder in the bubble motion response due to the acoustic forcing and the applied magnetic field.

Now, in order to compute the Lyapunov exponents, we need to transform the magnetic version of Rayleigh-Plesset equation in an autonomous system, given by Equation 17.

$$\begin{cases} \frac{dx}{dt} = y \\ \frac{dy}{dt} = \frac{1}{x}\left[-\frac{3}{2}y^2 + \frac{2}{We}\left(\frac{1}{x^3} - \frac{1}{x}\right)\right] - \frac{1}{x} - \frac{\varepsilon sin(\omega z)}{x} + \frac{1}{x^4} - \frac{4}{Re}\frac{y}{x^2} + \frac{1}{Re_{mag}}\left[\frac{\chi}{2}\left(ln(5) - ln(x) - \frac{3}{8}\right) - \frac{3}{32}\right] \\ \frac{dz}{dt} = 1 \end{cases} \tag{17}$$

Considering different values of Re, We, ε and the initial conditions it is possible to test the chaotic behavior of the bubble using a Matlab Lyaponov Exponents Toolbox. The output of the Matlab LET code (Siu, 1998) may give different behaviors, which can be classified as periodic cycles or stable equilibrium, non-linear chaotic and pure random processes. In this case, all the Lyapunov exponents are negative and the Lyapunov dimensions of the system is null. Therefore, the dynamic system is not chaotic.

In addition, another dynamical system analysis used less often, but extremely rich in information is the wavelet transform. Unlike FFT, which provides only information on the frequency, wavelets provide information in both time and frequency. In this case, the energy information is related to time and scales which correspond to the FFT frequencies. This analysis is interesting in order to visualize patterns. In particular, there is bidirectional energy information in two different spaces: time and frequency.

4.1 Neural Networks

For the trainning of both networks, the Scaled Conjugate Gradient method has been used in the Matlab Neural Network Toolbox. The basic conjugate gradient backpropagation algorithm adjusts the weights in the steepest descent direction (negative of the gradient). This is the direction in which the performance function is decreasing most rapidly. Even though the Scaled Conjugate Gradient needs more storage than the other second order algorithms, its convergence is more rapid. This algorithm is based upon a class of optimization techniques well known in numerical analysis as the Conjugate Gradient Methods (Moller, 1993). From an optimization point of view learning in a neural network is equivalent to minimizing a global error function, which is a multivariate function that depends on the weights in the network. This perspective gives some advantages in the development of effective learning algorithms because the problem of minimizing a function is well known in other fields of science, such as conventional numerical analysis (Watrous, 1987).

Considering the use of a logarithmic or tangential transfer function the results obtained by the neural network as patterns are not integer numbers and those errors can lead to misidentifications. For that approach, ten tests have been made for both harmonic and Lyapunov exponents inputs. In the case of the harmonic input, the FFT response containing both amplitude and frequency information from $\omega = 0$ to $\omega = 10$ are given as trainning set. For each case, the targets are given as the correct patterns. In the second network, using Lyapunov exponents, the input is given as the three exponents (LE_1, LE_2, LE_3) obtained from the autonomous system as shown in figure 5.

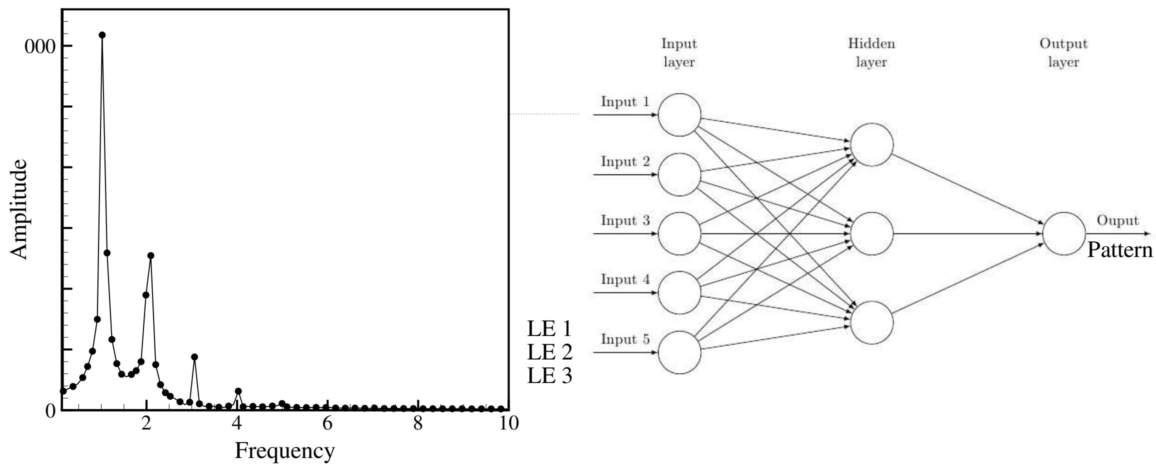

Figure 5: Typical schematic of a neural network.

For the first network, based on the frequency spectrum, 95 neurons are set in the hidden layer. The network is then trainned during 100 epochs for each test. In the first layer a logarithmic transfer function is used and in the second layer a linear transfer function. In the case of the second network, trainned with the Lyapunov exponents, 20 neurons are used on the hidden layer and the network was trainned for 1000 epochs. In the first layer a tangential transfer function has been used and in the second layer a linear transfer function.

4.1.1 Error Analysis

The performance of the pattern identification using Neural Networks is analyzed based on the normalized error. In this case, it is defined as the normalized absolute error between the identified pattern and the correct one:

$$E = \frac{|P_i - P_c|}{4} 100\% \tag{18}$$

where P_i is the pattern identified by the network, P_c is the correct pattern and 4 represents the number of possible patterns within the range of the physical parameters of the dynamical system explored.

In table 1 we can see an example related with three selected results between the ten tests performed. In this case, the higher relative error is 13.55%. Considering a bigger validation set, the error propagation is not going to be alarming. On the other hand, from table 2, we can see the larger relative error when using lyapunov exponents as the main information to train the neural network. Nevertheless, this information is not enough to decide which method would be better to use.

Table 1: Identified pattern and normalized error for the 3 of the 10 tests using the harmonic input.

	Test 1	Test 2	Test 3
Pattern 1	1.008 (0.2 %)	1.013 (0.33 %)	1.024 (0.60 %)
Pattern 2	1.905 (2.38 %)	1.795 (5.13 %)	1.729 (6.78 %)
Pattern 3	2.894 (2.65 %)	3.127 (3.18 %)	3.075 (1.88 %)
Pattern 4	4.237 (5.93 %)	4.135 (3.38 %)	3.967 (0.83 %)

We can see from figure 6 that even though the results from tables 1 and 2 have shown that the Lyapunov exponents can lead to more missidentifications, on the average, the results are more accurate and carry some relevant informations. The tests carried out here have demonstrated that the use of less information as input, such as the Lyapunov exponents, and more epochs of trainning may be more efficient. In this condition, the network has more time to adjust the neurons weights. In general, the patterns have small distinctions among themselves and the use of the frequency spectrum ends up not being the best tool. This is because the differences in bandwidth and amplitude of each harmonic do not change much. For this reason, the network ends up having difficulties in storing the primary characteristics of each pattern. If the patterns presented more non-linear characteristics as shown in other studies (Malvar *et al.*, 2015), the use of the frequency spectrum would be more appropriate.

Table 2: Identified pattern and normalized relative error for the 3 of the 10 tests using Lyapunov exponents input.

	Test 1	Test 2	Test 3
Pattern 1	1.335 (8.38 %)	1.387 (9.68 %)	1.430 (10.75 %)
Pattern 2	2.183 (4.58 %)	2.035 (0.88 %)	2.088 (2.20 %)
Pattern 3	3.099 (2.48 %)	2.906 (2.35 %)	3.118 (2.95 %)
Pattern 4	4.342 (8.55 %)	3.906 (2.35 %)	3.783 (5.43 %)

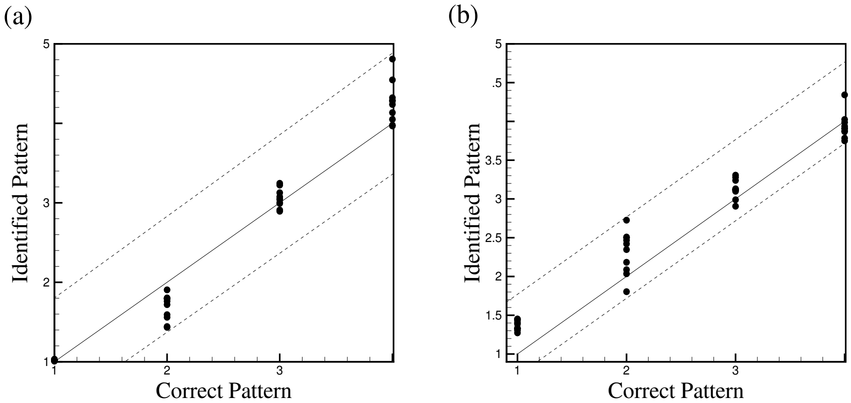

Figure 6: Comparison between both networks explored in the present work. (a) Result of 10 tests made with different weights initial conditions for the frequency spectrum input; (b) Results of 10 tests made with different weights initial conditions for the Lyapunov exponents input;

4.1.2 Pattern Identification

In order to consider the pattern identification the obtained pattern was rounded to an integer. trainned with the Lyapunov exponents. In this context, the higher the error obtained in the previous approach, the greater the chances for the neural network to misidentify the pattern (considering the rounding).

Table 3: Identified pattern for the 10 tests for the harmonic input. In this context, the neural network idenfity accurately the pattern in 90% of the time.

	Test 1	Test 2	Test 3	Test 4	Test 5	Test 6	Test 7	Test 8	Test 9	Test 10
Pattern 1	1	1	1	1	1	1	1	1	1	1
Pattern 2	2	2	2	1	2	2	2	2	1	2
Pattern 3	3	3	3	3	3	3	3	3	3	3
Pattern 4	4	4	4	5	5	4	4	4	4	4
Correct Identification	100 %	100 %	100 %	50 %	75 %	100 %	100 %	100 %	75 %	100 %

Table 4: Identified pattern for the 10 tests for the harmonic input. In this context, the neural network idenfity accurately the pattern in 95% of the time.

	Test 1	Test 2	Test 3	Test 4	Test 5	Test 6	Test 7	Test 8	Test 9	Test 10
Pattern 1	1	1	1	1	1	1	1	1	1	1
Pattern 2	2	2	2	3	2	2	2	2	3	2
Pattern 3	3	3	3	3	3	3	3	3	3	3
Pattern 4	4	4	4	4	4	4	5	4	4	4
Correct Identification	100 %	100 %	100 %	100 %	75 %	100 %	100 %	100 %	75 %	100 %

As we can see from tables 3 and 4, the Lyapunov exponents give a robust way for examining the bubble dynamic system explored in this work with neural network. The neural network correctly identified the vibrational pattern in 95 % of the time.

5. CONCLUSIONS

The present work has explored a method for identifying vibrational patterns in order to characterize the oscillatory motion of a spherical gas-bubble immersed in a magnetic fluid in the presence of an acoustic pressure forcing and an applied magnetic field. The motion of the bubble is governed by a magnetic version of the Rayleigh-Plesset equation.

For that we have considered that the bubble has no tangential deformation. This assumption is true for small bubbles under conditions of creeping flow. In this bubble size scale, the superficial tension forces are able to prevents deformation induced by inertial effects. Furthermore, it was noticed that under action of a magnetic field, the alignment of the particles tends to attenuate the amplitude of the bubble oscillatory motion. Consequently, less vibrational patterns are observed than in the case of the bubble immersed in a Newtonian fluid. These patterns have also shown greater periodicity. Nevertheless, the use of the fifth order Runge-Kutta method with adaptive time step and a criterion of collapse based on asymptotic theory for the minimum radius of collapse allowed the identification of smal anisotropy in both frequency spectrum and Lyapunov exponents.

In this situation frequency spectrum points and Lyapunov exponents have been employed in the training of neural networks. These neural networks were trained with the same algorithm: Scaled Conjugate Gradient method. Both presented very satisfactory results. During validation, the neural network trained with the amplitude and frequency information correctly identify the the vibrational pattern in 90% of the time. The network trained with Lyapunov exponents is even more efficient, resulting a 95% accuracy rate.

This is a consequence due to the fact that the network trained with the Lyapunov exponent has less information to be used in training (only 3 numbers), whereas in the case of frequency spectrum 95 points were used for each input. In addition, the exponents have been more sensitive to the changes of the patterns. This shows that the FFT may not be the most appropriated approach for this type of analysis in the absence of pattern being highly nonlinear. Indeed, from a practical point of view, changes in harmonics amplitude is not very significant in these cases.

In pratical problems that make use of the cavitation phenomena and ferrofluids, this identification opens application possibilites in different fields, such as biomedical and naval industries. In the cavitation study, characterizing the bubble freedom degrees in its nonlinear motion is very important for predicting premature collapse. In this context, using neural networks in order to identify cavitation vibration modes seems to be very promising for a complete characterization of bubble dynamics.

6. ACKNOWLEDGEMENTS

The authors would like to thank CAPES and CNPq to the partial financial support on the conduction of this study.

7. REFERENCES

Albernaz, D.L. and Cunha, F.R., 2011. "Bubble dynamics in a maxwell fluid with extensional viscosity". *Mechanics Research Communications*, Vol. 38/3, p. 255.

Bacri, J.C. and Salin, D., 1982. "Instability of ferrofluid magnetic drops under magnetic field." *J of Physique Lettres*, Vol. 43(17), pp. 649–654.

Bashtovoi, V., Kuzhit, P. and Reks, A., 2002. "Capillary ascension of magnetic fluids". *J. Magn. Magn. Mater.*, Vol. 252, pp. 265–267.

Bolshakova, I., Bolshakov, M., Zaichenko, A. and Egorov, A., 2005. "The investigation of the magnetic fluid stability using the devices with magnetic field microsensors." *J of Magnetism and Magnetic Materials*, Vol. 289, pp. 108–110.

Brujan, E.A., 1999. "A first-order model for bubble dynamics in a compressible viscoelastic liquid". *J Non-Newtonian Fluid Mech.*, Vol. 84, pp. 83–103.

Brusentsov, N.A., Brusentsova, T.N., Filinova, E.Y., Pirogov, Y.A., Kupriyanov, D.A., Dubina, A.I., Shumskikh, M.N., Shumakov, L.I., Yurchenko, N.Y., Anashkina, E.A. and Shevelev, A.A., 2008. "Magnetohydrodynamic thermochemoterapy of malignant tumors with nanopreparations with magnetic resonance monitoring". *Pharm. Chem. J.*, Vol. 42(4).

Chahine, G.L., 1982. "Experimental and asymptotic study of nonspherical bubble collapse". *Applied Scientific Research*, Vol. 38, pp. 187–197.

Cunha, F.R., Souza, A.J. and Morais, P.C., 2002. "The dynamic behavior of a collapsing bubble in a magnetic fluid". *J. of Magnetism and Magnetic Materials*, Vol. 252, pp. 271–275.

Gontijo, R.G. and Cunha, F.R., 2012. "Experimental investigation on thermo-magnetic convection inside cavities". *J. Nanosci. Nanotechnol.*, Vol. 12, pp. 9198–9207.

Gontijo, R.G. and Cunha, F.R., 2015. "Dynamic numerical simulations of magnetically interacting suspensions in creeping flow". *Powder Technology*, Vol. 279, pp. 146–165.

Johnsen, E. and Colonius, T., 2009. "Numerical simulations of non-spherical bubble collapse". *J Fluid Mechanics*, Vol. 629, pp. 231–262.

Laplace, P.S.M., 1805. *Traité de Mécanique Céleste*. Paris, France.

Malvar, S., Cunha, F.R. and Gontijo, R.G., 2015. "Vibrational modes on the non-linear motion of an oscillating bubble in a newtonian fluid using neural networks". *DINAME 2015 - Proceedings of the XVII International Symposium on Dynamic Problems of Mechanics*, Vol. ABCM, Natal, RN, Brazil.

Moller, M.F., 1993. "A scaled conjugate gradient algorithm for fast supervised learning". *Neural networks*, Vol. 6(4), pp. 525–533.

Odenbach, S., 2002. *Ferrofluids, Magnetically Controllable Fluids and Their Applications.* Springer, Berlin.

Rosensweig, R.E., 1987. "Magnetic fluids." *Ann. Rev. Fluid Mech*, Vol. 19, pp. 437–463.

Siu, S., 1998. "Lyapunov exponents toolbox (let)".

Soh, W.K. and Karimi, A.A., 1996. "On the calculation of heat transfer in a pulsating bubble". *Math Modell*.

Watrous, R.L., 1987. "Learning algorithms for connectionist networks: Applied gradient methods of nonlinear optimization". *Proc. IEEE 1st International Conference on Neural Networks*, Vol. 2, pp. 619–628.

Young, T., 1805. "An essay on the cohesion of fluids". *Philosophical Transactions of the Royal Society of London*, Vol. 95, pp. 65–87.

Zahn, M., 2001. "Magnetic fluid and nanoparticle applications to nanotechnology." *J of Nanoarticle Research*, Vol. 3, pp. 73–78.

Zharov, V.P., Letfullin, R.R. and Galitovskaya, E.N., 2005. "Microbubbles-overlapping mode for laser killing of cancer cells with absorbing nanoparticle clusters". *J of Physics D: Applied Physics*, Vol. 38, pp. 2571–2581.

8. RESPONSIBILITY NOTICE

The authors are the only responsible for the printed material included in this paper.